Research Article Vol. 36, No. 10 / October 2019 / Journal of the Optical Society of America B 2907

Journal of the Optical Society of America B

OPTICAL PHYSICS

Photothermal mirror Z-scan spectrometry of opaque samples

ARISTIDES MARCANO OLAIZOLA

Division of Physics, Engineering, Mathematics, and Computer Science, Delaware State University, 1200 North DuPont Highway, Dover, Delaware 19901, USA (amarcano@desu.edu)

Received 8 July 2019; revised 4 September 2019; accepted 4 September 2019; posted 4 September 2019 (Doc. ID 372066); published 1 October 2019

This contribution introduces a pump-probe photothermal mirror Z-scan method to measure the thermal quantum yield, the thermal diffusivity, and other photothermal parameters of an opaque solid. The focusing of a pump beam of light onto the sample generates thermoelastic surface distortions. The distorted surface acts as a mirror affecting the diffraction pattern of a reflected probe beam yielding the experimental signal. Scanning the focusing lens produces a single peak photothermal mirror Z-scan signature. The amplitude and time evolution of the signal determines the sample's photothermal properties. The method is used to analyze gallium arsenide and silicon plates, obtaining good agreement with previous studies.

https://doi.org/10.1364/JOSAB.36.002907

1. INTRODUCTION

The focusing of a beam of light onto a material releases local heat following the absorption of light photons by the atoms of the first layers of the sample's surface. The released heat distorts the surface locally due to the thermoelastic effect yielding to the formation of a nanometric bump or photothermal mirror (PTM) [1,2]. The PTM affects the wavefront of any reflected light. A probe beam of light, whose spot area is much larger than that of the pump beam, tests the PTM. The diffraction pattern of the reflected probe beam at the far field exhibits significant distortions. Measuring the relative transmission of the probe light through a small aperture centered at the probe beam spot generates the experimental signal. The concurrent resolution of the equation for thermoelastic deformation and the equation for thermal diffusivity provides a theoretical model to explain the PTM effect. The approach shows that the PTM signal is proportional to the quantum thermal yield of the surface defined as a relative amount of the absorbed energy used to generate heat. The method allows the study of thermoelastic properties and photothermal parameters of transparent and non-transparent samples [3–13].

This work introduces a pump-probe Z-scan variation of the technique, which allows effective calibration procedures. We focus a previously collimated pump beam over the sample to create the PTM. By scanning the lens around the focal point, we generate PTMs of different magnitudes. We use a collimated probe beam with a spot diameter of few millimeters, which does not change during the experiment. The distance between the sample and the detection plane is also fixed. The signal is maximal at the pump focal point and diminishes for larger dimension pump beam spots resulting in a single peak Z-scan signature. The amplitude of the peak measures the total PTM phase shift bearing information about the thermal quantum yield and the thermoelastic properties of the sample. The technique provides the value of the sample's thermal diffusivity coefficient by analyzing the time evolution of the signal. The experiment exhibits several advantages comparing to the conventional PTM technique with a fixed lens position. First, the Z-scanning allows the identification of the location for the maximal signal.

On the other hand, the half wave half maximum (HWHM) of the Z-scan peak defines the Rayleigh range of the pump beam in the bulk of the material in a similar way it is done in a conventional Z-scan experiment [14,15]. This parameter defines the dimensions of the pump beam spot within the sample, the PTM time buildup, and the mode-mismatched parameter, which are crucial data to complete a reliable fitting procedure. The procedure fits only the values of the pump beam Rayleigh range and the PTM phase shift amplitude. The rest of the parameters have fixed values determined by the conditions of the experiment. The pump beam Rayleigh range is generally difficult to estimate if no Z-scanning is conducted yielding to substantial uncertainties. Additionally, the Z-scan method opens the possibility of the study of other non-linear effects since the phenomena of different physical origins should have different Z-scan responses.

The work validates the method by studying the PTM Z-scan response of a gallium arsenide (GaAs) plate and a silicon wafer (Si wafer). Thanks to their significant importance for the solar energy and electronics industry, the characteristics of these

materials are well known [16–20]. Their study allows validation and calibration of the proposed PTM Z-scan technique. Analysis of the PTM Z-scan determines the values of the thermal quantum yields of the GaAs plate and the Si wafer, namely a measure of the ability of the samples to generate heat upon interaction with light. For photovoltaic applications, it is convenient to keep the thermal quantum yield small. Photothermal applications require high thermal quantum yield values. A thermal quantum yield of one means that 100% of the absorbed energy turns into heat. The method allows a remote spectral analysis of impurities deposited over the sample's surface as well as for monitoring of its thermoelastic, thermal diffusivity, and other thermo-optical properties.

2. THEORY

Different authors have discussed the theoretical model that describes the PTM effect [3–13]. The concurrent resolution of the thermal diffusivity and thermoelasticity equations yields the theoretical approach. The absorption of the pump light injects heat onto the surface inducing thermoelastic deformations. Thermal diffusivity acts as a compensation mechanism by spreading the heat over the surface. Over time, the thermoelastic strain reaches a stationary distribution. The presence of the PTM affects the wavefront of the reflected probe beam. PTM is different from the well-known thermoreflectance technique. The temperature changes modify the reflectivity of the surface. However, reflectivity changes affect mostly the amplitude of the reflected field and not its phase. The contribution of the amplitude changes on the diffraction pattern at the far field is negligible compared to the phase changes induced by the PTM. We measure the transmission of the reflected probe beam through a small aperture located at the far field and centered on the beam's central spot. The dimension of the aperture is much lower than the radius of the reflected probe beam at the detection plane. We define the PTM signal as

$$S(z,t)=\left|\frac{I(z,t)-I(z,0)}{I(z,0)}\right|, \tag{1}$$

where

$$I(z,t)=I_o\left|\int_0^{\infty}\exp(-(1+iV)g-i\Delta\Phi(g,z,t)dg\right|^2 \tag{2}$$

is the intensity of the probe light at the center of the beam spot, I_o is a constant, $V=z_1/z_p+z_p[(z_1/z_p)^2+1]/d$ is the Fresnel parameter, z_1 is the distance from the probe beam waists to the sample, z_p is the Rayleigh range of the probe beam, d is the distance from the sample to the detection plane, $g=(r/a_p)^2$, a_p is the radius of the probe beam at the sample, r is the transversal coordinate on the surface of the sample, t is the time, z is the distance between the lens and the sample surface, and $\Delta\Phi(g,z,t)$ is the phase shift induced by the presence of the PTM. A converging lens focuses the pump beam onto it. We consider this beam to be Gaussian with Rayleigh parameter z_e. For opaque samples (high absorption) the phase is [5]

$$\Delta\Phi(g,z,t)=\Phi_o\int_0^{\infty}\exp(-\eta^2/8)\,f(\eta,z,t)J_o\times\left(\eta\sqrt{g\,m(z)}\right)d\eta, \tag{3}$$

where

$$f(\eta,z,t)=\frac{\eta t}{t_c(z)}Erfc\left(\eta\sqrt{\frac{t}{4t_c(z)}}\right)-2\sqrt{\frac{t}{\pi\,t_c(z)}}\times\exp\left(-\eta^2\frac{t}{4t_c(z)}\right)+\frac{2}{\eta}Erf\left(\eta\sqrt{\frac{t}{4t_c(z)}}\right), \tag{4}$$

$$\Phi_o=-P_e\cdot(1-R)\cdot\psi\cdot\alpha_T\cdot(1+\nu)/\left(\lambda_p\kappa\right) \tag{5}$$

is the amplitude of the phase shift, J_o is the Bessel function of zero order, $m(z)=(a_p/a(z))^2$ is the mode-mismatched parameter, $a(z)=a_e(1+z^2/z_e^2)^{0.5}$, a_e is the pump beam radius at the beam waist, which is related to the Rayleigh range according to $z_e=\pi n a_e^2/\lambda_e$, n is the sample's refraction index, λ_e is the pump light wavelength, λ_p is the probe beam wavelength, P_e is the power of the pump light, κ is the sample's thermal conductivity, $t_c(z)=a(z)^2/(4D)$ is the thermal mirror buildup time, D is the thermal diffusivity coefficient, α_T is the thermoelastic coefficient, R is the reflectivity at the pump wavelength, ψ is the fraction of the absorption converted into heat or thermal quantum yield, and ν is the Poisson ratio. The model shows that the signal $S(t)$ is linearly proportional to Φ_o for small phase values (see discussion below).

The Z-scan PTM experiment consists of scanning the lens, which focuses the pump beam generating different beam spot dimensions over the sample's surface. The sample remains in a fixed position. We define the zero of the longitudinal coordinate z as the position of the lens, which provides the maximal focusing. An independent optics directs a collimated probe beam toward the same point on the surface under a small angle to the direction of the pump field. Thus, the probe beam spot's dimension remains also fixed. This experimental configuration yields a single peak Z-scan response. Mathcad software resolves Eqs. (1)–(5) using parameters close to those used in the experimental section.

Figure 1 shows the results of the Z-scan signal calculation using Eqs. (1)–(5) with parameters $n=3.42$, $\lambda_p=632$ nm, $\lambda_e=532$ nm, $d=220$ m, $a_p=0.15$ cm, $D=0.5$ cm^2 s^{-1}, $\Phi_o=-0.016$, and three different pump beam Rayleigh ranges $z_e=0.032$ cm, 0.129 cm, and 0.291 cm as indicated in the figure. The phase is negative, which is consisting of a defocusing PTM mirror. The thermal diffusivity corresponds to a silicon wafer [18]. The peak amplitude occurs for the maximal focusing. Its value is independent of the Rayleigh range. The Rayleigh range determines the width of the peak. The inset figure shows that the full width half-maximum of the Z-scan peak is linearly proportional to the square root of the pump beam Rayleigh range, at least for the values chosen for the numerical simulation. The model shows that the value of Φ_o does not affect the shape of the Z-scan curves. The value of D does not affect the curve either.

Figure 2 shows the Z-scan curves calculated using Eqs. (1)–(5) for $z_e=0.03$ cm and different Φ_o values: −0.01,

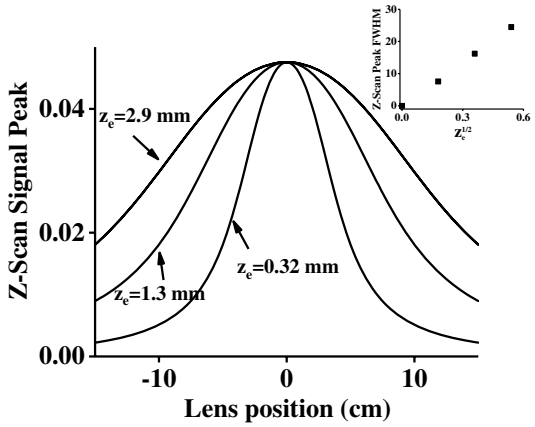

Fig. 1. PTM Z-scan signal calculated using Eqs. (1)–(5) and the following parameters: $\lambda_e = 532$ nm, $\lambda_p = 632$ nm, $n = 3.42$, $D = 0.88$ cm^2 s^{-1}, $d = 220$ cm, $z_p = 3800$ cm, $\phi_o = -0.016$, $t = 0.05$ s, and for $z_e = 0.032$, 0.13, and 0.29 cm. The inset shows the full width half-maximum (FWHM) of the Z-scan peak as a function of the square root of the Rayleigh range z_e.

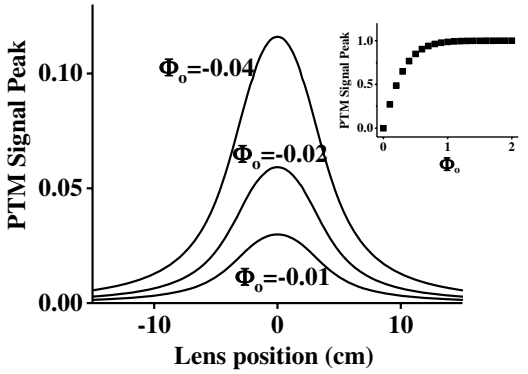

Fig. 2. PTM Z-scan signal calculated using Eqs. (1)–(5) and the following parameters: $\lambda_e = 532$ nm, $\lambda_p = 632$ nm, $n = 3.42$, $D = 0.88$ cm^2 s^{-1}, $d = 220$ cm, $z_p = 3800$ cm, $z_e = 0.03$ cm, and $\Phi_o = -0.01$, -0.02, and -0.04. The inset figure shows the dependence of the maximal value of the PTM signal as a function of Φ_o.

-0.02, and -0.04. The rest of the parameters are as in Fig. 1. The width of the peak does not change with Φ_o. For small Φ_o, the maximal amplitude is linearly proportional to Φ_o. The inset of the figure shows the dependence of the peak amplitude on Φ_o. The numerical study shows that the linear proportionality between the signal peak and Φ_o is a good approximation for $|\Phi_o| < 0.3$. For larger Φ_o, the model predicts the signal saturation, which approaches asymptotically the value of one. It corresponds to the total light depletion at the center of the probe beam.

Figure 3 shows the maximal PTM signal as a function of time for different thermal diffusivity values: $D = 0.1$ cm^2 s^{-1}, 0.31 cm^2 s^{-1}, and 0.88 cm^2 s^{-1}. The rest of the parameters are as in Figs. 1 and 2. The signal exhibits a fast growth during the first millisecond of the interaction followed by a slow asymptotically approach to a stationary value. In this situation, the thermal diffusivity compensates the intake of energy due to the

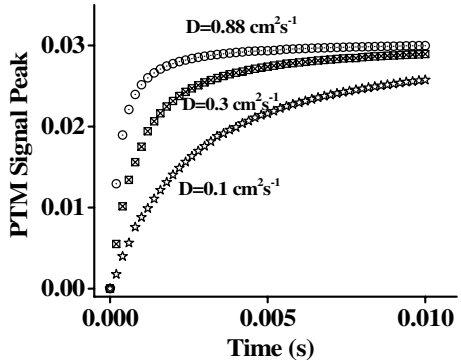

Fig. 3. Maximal value of the PTM signal as a function of time calculated using Eqs. (1)–(5). $D = 0.1$, 0.3, and 0.88 cm^2 s^{-1}. The rest of the parameters are as in Fig. 1.

absorption of light, and the PTM reaches a stationary shape. As the value of D increases, the transition to the stationary regime accelerates. The numerical model shows that the pump Rayleigh range and Φ_o values do not affect the time dependence. Thus, the theoretical fitting of the time evolution data yields the value for the sample's thermal diffusivity coefficient.

3. EXPERIMENT

Figure 4 shows a simplified scheme of the Z-scan PTM experiment. A 200 mW 532 nm diode-pumped solid-state (DPSS) laser generates the pump beam. A signal generator modulates the pump beam typically between 1 and 200 Hz. A small glass plate (B) redirects part of this light to a detector (D_R) used for reference purposes. A telescope (C_2) collimates the pump beam to a parallel beam of 4 mm diameter. A 20 cm lens L focuses the pump beam onto the sample creating on its surface the PTM. Scanning of the focusing lens along the longitudinal z-direction yields the Z-scan signature. A 2 mW CW He laser (632 nm) provides the probe light to test the PTM. Another telescope (C_1) collimates the probe beam extending its diameter up to 6 mm. The mirror M_1 redirects the collimated probe beam toward the sample covering the spot of the focused pump beam. The mirror M_2 collects the reflected probe beam of light and redirects it toward an aperture A. The mirror centers the probe beam to the

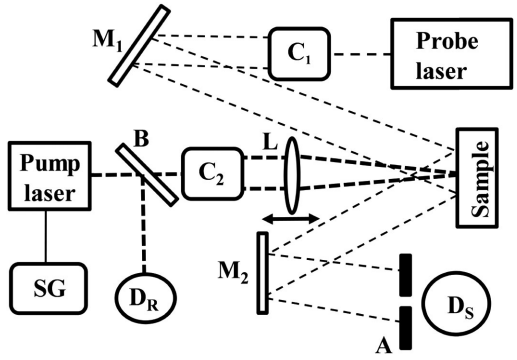

Fig. 4. Experimental setup consisting of a pump laser modulated by an external signal generator (SG), a beam splitter B, a reference semiconductor detector D_r, a sample, a pump beam collimator C_2, a focusing lens L, a probe laser, a probe beam collimator C_1, mirrors M_1 and M_2, an aperture A, and a signal semiconductor detector D_s.

Table 1. Thermophysical and Optical Parameters of GaAs and Si Wafer

Parameter	GaAs Plate	Si Wafer
Thermal diffusivity D ($cm^2\ s^{-1}$)	0.31 [19]	0.5 [18]
Thermal conductivity κ ($Wcm^{-1^\circ}\ K^{-1}$)	0.55 [19]	1.56 [16]
Thermoelastic coefficient α_T ($^\circ K^{-1}$)	5.7310^{-6} [19]	2.610^{-6} [17]
Poisson ratio ν	0.31 [20]	0.22 [20]
Refractive index n	3.66 [20]	3.42 [20]
Reflectivity R	0.07	0.4
Φ_o at 156 mW of 532 nm radiation	$0.031\Psi_{GaAs}$	$0.30\Psi_{Si}$

aperture. Behind the aperture, a semiconductor diode records the transmitted probe light. The signal is pre-amplified and sent to a digital oscilloscope for processing. The time evolution of the signal is collected at the focal position ($z = 0$).

The experiments measure the PTM Z-scan responses of a GaAs plate and a Si wafer. The GaAs plate has a thickness of 1 mm and a surface of about $1cm^2$. The Si wafer is circular with a radius of 2 cm and thickness of 1 mm. The plates have one side polished with good optical quality. Direct measurement of the reflectivity at 532 nm provides values of 0.07 and 0.4 for the GaAs plate and the Si wafer, respectively. Both samples are non-transparent for the pump and probe light in correspondence to their high absorption at 532 and 632 nm. The low reflectivity of the GaAs plate is due to the presence of an antireflection coating. The experimental section shows that the presence of the coating does not affect the obtained good agreement between the predictions of the model and the experiments.

In Table 1, we show the thermal diffusivity, thermal conductivity, thermoelastic coefficients, Poisson ratios, and refraction coefficients of the GaAs and Si, which have been reported elsewhere [16–20]. Table 1 includes the values of the measured reflectivity and the expected PTM Φ_o for 156 mW of pump radiation power calculated using Eq. (5) and the photothermal parameters indicated in the table. The Φ_o values are expressed in terms of the photothermal quantum yields Ψ_{GaAS} and Ψ_{Si}, which measure the relative amount of the absorbed energy used to generate heat for the GaAs and the Si wafer, respectively. The photothermal quantum yield will be estimated from the experiments below. If $\Psi_{GaAS} \approx \Psi_{Si}$, the estimation concludes that the PTM signal of GaAs should be at least an order of magnitude larger than that of the Si wafer.

4. RESULTS

Figure 5(a) shows the Z-scan PTM signal of the GaAS plate obtained when using 156 mW of the 532 nm radiation from a DPSS laser as pump light. In this experiment, the signal generator modulates the laser at a frequency of 10 Hz.

The solid line corresponds to a fitting performed using Eqs. (1)–(5), and parameters $\lambda_p = 632$ nm, $z_e = 0.027$ cm, $a_p = 0.3$ cm, $D = 0.31\ cm^2\ s^{-1}$, $d = 220$ cm, $D = 0.31\ cm^2\ s^{-1}$, $\Phi_o = -0.027$, and $t = 0.05$ s. The parameters λ_p, d, a_p, and t are taken from the experimental conditions. The parameter D is taken from Table 1. The fitting procedure generates the values of z_e and Φ_o. Using the obtained value of z_e, the value $n = 3.66$ from Table 1, and $\lambda_e = 532$ nm, we estimate $a_e = 3.5$ μm. Using the value of Φ_o and using Table 1, we obtain a photothermal quantum yield of $\Psi_{GaAs} = 0.87$ at 532 nm. Thus, most of the energy absorbed from photons goes to the generation of heat. The value agrees well with the recently published results obtained using the regular PTM spectrometry [21]. Figure 5(b) shows the time dependence of the maximal PTM signal for GaAs measured under the same experimental conditions. The high experimental signal-to-noise ratio obtained confirms the high sensitivity of the photothermal approach [12–15]. The numerical calculation performed using Eqs. (1)–(5) using the same parameters as in Fig. 5(a) yields the solid white line. The results confirm a good agreement between the experiments and the predicted by the model results.

Figure 6(a) shows the results of the Z-scan PTM signal of the Si wafer under the same experimental conditions of Fig. 5(a). The solid line is the theoretical fitting obtained solving Eqs. (1)–(5) with parameters $\lambda_p = 632$nm, $z_e = 0.03$cm, $a_p = 0.3$cm, $d = 220$cm, $D = 0.52cm^2s^{-1}$, $\Phi_o = -0.0021$, and $t = 0.05$s. The parameters λ_p, d, a_p, and t are taken from the experimental conditions. The parameter D is taken from Table 1. The fitting procedure generates the values of z_e and

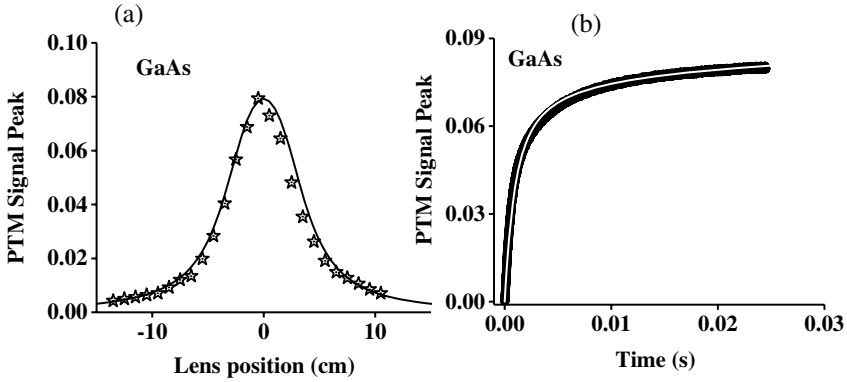

Fig. 5. (a) PTM Z-scan curve of the GaAs plate obtained using 156 mW of 532 nm radiation. The black solid line is the fitting of the data calculated using Eqs. (1)–(5) and the following parameters: $\lambda_e = 532$ nm, $\lambda_p = 632$ nm, $n = 3.66$, $D = 0.31\ cm^2\ s^{-1}$, $d = 220$ cm, $z_p = 3800$ cm, $\Phi_o = -0.027$, $t = 0.05$ s, and $z_e = 0.027$ cm. (b) Time dependence of the maximal PTM signal from the GaAs plate; the solid white line is the fitting of the data obtained using the same parameters as in (a).

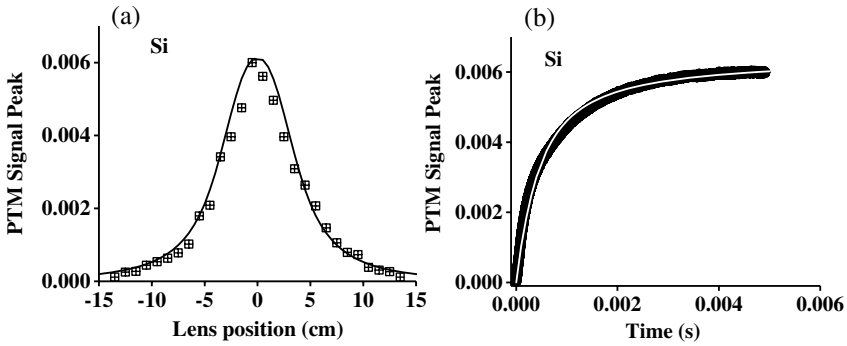

Fig. 6. (a) PTM Z-scan curve of the Si wafer obtained using 156 mW of 532 nm radiation. The black solid line is the fitting of the data calculated using Eqs. (1)–(5) and the following parameters: $\lambda_e = 532$ nm, $\lambda_p = 632$ nm, $n = 3.42$, $D = 0.52$ cm^2 s^{-1}, $d = 220$ cm, $z_p = 3800$ cm, $\phi_o = -0.0021$, $t = 0.05$ s, and $z_e = 0.027$ cm. (b) Time dependence of the maximal PTM signal from the Si wafer; the solid white line is the fitting of the data obtained using the same parameters as in (a).

Φ_o. Using the obtained value of z_e, the value of $n = 3.42$ from Table 1, and $\lambda_e = 532$ nm, we estimate $a_e = 3.8$ μm. As expected according to Table 1, the Si wafer PTM signal is much smaller than the signal for the GaAs sample. However, the sensitivity of the experiment still provides a good signal-to-noise ratio. The fitting yields $\Psi_{Si} = 0.7$ at 532 nm. Figure 6(b) shows the time dependence of the PTM signal of the Si wafer. The solid white line corresponds to the predictions of the model using Eqs. (1)–(5) and the same parameters as in Fig. 6(a).

5. CONCLUSIONS

The work describes a pump-probe PTM Z-scan technique aimed at the photothermal characterization of opaque reflective plates. The PTM study provides information about the thermoelastic coefficient, the thermal diffusivity coefficient, and the photothermal quantum yield. An interpretation based on the concurrent resolution of the equations ruling the thermal diffusion and the thermoelastic deformations explains the basic properties and applicability of the method. PTM spectrometry of a GaAs plate and a Si wafer, which are materials commonly used for solar energy and electronic applications, validates the theoretical model. The comparison between theory and experiments provides thermal quantum yield values of 0.85 and 0.7 for the GaAs plate and the Si wafer, respectively.

Funding. Directorate for Education and Human Resources (1719379, 1744502, 1831332); National Science Foundation (NSF).

Acknowledgment. The author thanks Sol-Ideas for providing the GaAs and the Si wafer samples.

Disclosures. The author declares that there are no conflicts of interest related to this article.

REFERENCES

1. P. Kuo and M. Munidasa, "Single-beam interferometry of a thermal bump," Appl. Opt. **29**, 5326–5331 (1990).
2. B. Li, Z. Zhen, and S. He, "Modulated photothermal deformation in solids," J. Phys. D **24**, 2196–2201 (1991).
3. T. Elperin and G. Rudin, "Thermal mirror method for measuring physical properties of multilayered coatings," Int. J. Thermophys. **28**, 60–82 (2007).
4. N. G. C. Astrath, L. C. Malacarne, P. R. B. Pedreira, A. C. Bento, M. L. Baesso, and J. Shen, "Time-resolved thermal mirror for nanoscale surface displacement detection in low absorbing solids," Appl. Phys. Lett. **91**, 191908 (2007).
5. F. Sato, L. C. Malacarne, P. R. B. Pedreira, M. P. Belancon, R. S. Mendes, M. L. Baesso, N. G. C. Astrath, and J. Shen, "Time-resolved thermal mirror method: A theoretical study," J. Appl. Phys. **104**, 053520 (2008).
6. L. C. Malacarne, F. Sato, P. R. B. Pedreira, A. C. Bello, R. S. Mendes, M. L. Baesso, N. G. C. Astrath, and J. Shen, "Nanoscale surface displacement detection in high absorbing solids by time-resolved thermal mirror," Appl. Phys. Lett. **92**, 131903 (2008).
7. L. C. Malacarne, N. G. C. Astrath, G. V. B. Lukasievicz, E. K. Lenzi, M. S. Baesso, and S. Bialkowski, "Time-resolved thermal lens and thermal mirror spectroscopy with sample-fluid heat coupling: A complete model for material characterization," Appl. Spectrosc. **65**, 99–104 (2011).
8. V. S. Zanuto, L. S. Herculano, M. S. Baesso, G. V. B. Lukazievicz, C. Jacinto, L. C. Malacarne, and N. G. C. Astrath, "Thermal mirror spectrometry: an experimental investigation of optical glasses," Opt. Mater. **35**, 1129–1133 (2013).
9. N. G. C. Astrath, L. C. Malacarne, V. S. Zanuto, M. P. Belancon, R. S. Mendes, M. L. Baesso, and C. Jacinto, "Finite size effect on the surface deformation thermal mirror method," J. Opt. Soc. Am. B **28**, 1735–1739 (2011).
10. G. V. B. Lukasievicz, L. C. Malacarne, N. G. C. Astrath, V. S. Zanuto, L. S. Herculano, and S. E. Bialkowski, "A theoretical and experimental study of time-resolved thermal mirror with non-absorbing heat-coupling fluids," Appl. Spectrosc. **66**, 1461–1467 (2012).
11. O. S. Arestegui, P. Y. N. Poma, L. S. Herculano, G. V. B. Lukasievicz, F. B. Guimaraes, L. C. Malacarne, M. L. Baesso, S. E. Bialkowski, and N. G. C. Astrath, "Combined photothermal lens and photothermal mirror characterization of polymers," Appl. Spectrosc. **68**, 777–783 (2014).
12. A. Marcano, G. Gwanmesia, M. King, and D. Caballero, "Determination of thermal diffusivity of opaque materials using the photothermal mirror method," Opt. Eng. **53**, 127101 (2014).
13. A. Marcano, G. Gwanmesia, and B. Workie, "Photothermal mirror method for the study of thermal diffusivity and thermo-elastic properties of opaque solid materials," Int. J. Thermophys. **38**, 136 (2017).
14. A. Marcano, C. Loper, and N. Melikechi, "High sensitivity absorption measurement in water and glass samples using a mode-mismatched pump-probe thermal lens method," Appl. Phys. Lett. **78**, 3415–3417 (2001).
15. A. Marcano, C. Loper, and N. Melikechi, "Pump probe mode mismatched Z-scan," J. Opt. Soc. Am. B **19**, 119–124 (2002).

16. H. R. Shanks, P. D. Maycock, P. H. Sidles, and G. C. Danielson, "Thermal conductivity of silicon from 300 to 1400°K," Phys. Rev. **130**, 1743–1748 (1963).
17. Y. Okada and Y. Tokumaru, "Precise determination of lattice parameter and thermal expansion coefficient of silicon between 300 and 1500 K," J. Appl. Phys. **56**, 314–320 (1984).
18. https://www.netzsch-thermal-analysis.com/us/materials-applications/photovoltaics/silicon-wafer-thermophysical-properties.
19. "Thermal of gallium arsenide," http://www.ioffe.ru/SVA/NSM/Semicond/GaAs/thermal.html.
20. S. M. Sze, *Semiconductor Sensors* (Wiley, 1994), Appendix D, p. 535.
21. P. P. González-Borrero, G. V. B. Lukasievicz, V. S. Zanuto, N. G. C. Astrath, and L. C. Malacarne, "Accessing thermo-mechanical properties of semiconductors using a pump-probe surface displacement method," J. Appl. Phys. **121**, 195101 (2017).